7
Photovoltaics: Light-Trapping in Crystalline Silicon and Thin-Film Solar Cells by Nanostructured Optical Coatings

Pierpaolo Spinelli,[1] Bonna K. Newman,[1] and Albert Polman[2]

[1]Energy Research Centre of the Netherlands, Solar Energy Unit, Westerduinweg 3, 1755 LE Petten, The Netherlands
[2]FOM Institute AMOLF, Center for Nanophotonics, Science Park 104, 1098 XG, Amsterdam, The Netherlands

7.1 Introduction

Nanostructures can be used to improve the performance of solar cell devices. The strong scattering of light resulting from optical resonances of both metallic and dielectric nanostructures can be used to efficiently couple and trap light in a solar cell device [1–3]. The nature of the optical resonance in metal and dielectric nanoparticles (NPs) is very different due to the intrinsic difference in the optical constants of the two classes of materials. Optically, metal NPs are characterized by localized surface plasmon resonances (LSPRs), which originate from the collective excitation of the free electrons in the metal by the electric field of the incident light [4]. At resonance, the field is confined to the NP surface. Dielectric nanoparticles, on the other hand, possess geometrical resonances where light is confined to well-defined geometrical modes inside the NP [5]. These latter are usually referred to as Mie resonances, after the German physicist Gustav Mie (1869–1957) who first solved Maxwell's equations for a plane wave incident on a spherical particle in a homogeneous medium [6].

Despite the different physics behind the optical resonances in plasmonic and Mie resonant NPs, two key mechanisms governing the scattering properties of both kinds of NPs are beneficial for solar cell applications. First, both kinds of resonant NPs are characterized by a scattering cross section larger than the NP area. It has been shown that this allows full interaction of the NPs with the incident light even if an array with less than 30% surface coverage is used [7,8]. Second, the scattered light is directed preferentially toward the materials with higher refractive index, due to the higher density of optical states [9,10]. This

Nanotechnology for Energy Sustainability, First Edition. Edited by Baldev Raj, Marcel Van de Voorde, and Yashwant Mahajan.

effect can be used to enhance the absorption of light in solar cells based on high-index semiconductors.

The strong optical scattering allows improvement of the absorption of light in the solar cell and thus photocurrent generation. This effect is beneficial for the cell short-circuit current density (J_{sc}). Besides the enhanced current generation, nanostructures can also be beneficial for efficient current extraction from the cell. For example, the use of nanostructures instead of standard textures enables the realization of novel solar cell design in which both surfaces are flat, and surface recombination is reduced [11]. This has a beneficial effect on the cell open-circuit voltage (V_{oc}). Moreover, metal nanostructures can also be interconnected and be used as an electrode for the solar cell device. For example, Ag nanowire networks can be used as a transparent conductive electrode as an alternative to standard transparent conductive oxides (TCOs). The efficient current extraction could also decrease the series resistance and improve the fill-factor (FF) of the cell [12].

Various configurations of metal and dielectric nanoparticles have been studied for different types of solar cells. They include designs in which NPs are placed at the front [13–16], at the back [17–21], or inside the solar cell active layer [22–26]. Silicon substrates have been the most used platform both to study the fundamentals of the resonant light scattering by nanoparticles into a substrate and to show the improvements on cell performance. However, the preferential scattering of light by resonant nanoparticles can be used to enhance light in-coupling into any high-index material. This includes thin-film cells devices such as GaAs, CdTe, or CIGS solar cells. Furthermore, solar cells also based on low-refractive-index materials (such as organic or perovskite solar cells) can benefit from light gathering properties of nanoparticles. For example, the near-field enhancement provided by metal nanoparticles embedded in organic layers has been shown to improve the light absorption of the layer [22–24]. However, this usually comes at the expense of parasitic losses in the metal [27,28].

In this contribution, we give an overview of different ways by which resonant nanostructures can be used to improve solar cells. We analyze the benefits and drawbacks of applying front-side nanostructured coatings to a wide variety of solar cell designs. The chapter is organized as follows:

- In Section 7.2, we present and compare different crystalline Si solar cell designs that can benefit from nanostructured coatings, from the point of view of both light absorption (J_{sc}) and surface passivation (V_{oc}). A summary table of the properties of different nanostructured coatings is provided.
- In Section 7.3, we present the application of resonant nanostructures to thin-film solar cell devices. The examples of high-efficiency GaAs solar cells and inexpensive polymer solar cells are presented.
- Section 7.4 gives an overview of other nanostructures concepts that allow improving the solar cell performance, including metal nanowire network electrodes, rear-side nanostructured reflectors, and new antireflection approaches for module glass.

7.2
Crystalline Si Solar Cells

The photovoltaic market is currently dominated by monocrystalline or polycrystalline Si solar cells [29]. Furthermore, c-Si based modules have the highest efficiencies among single-junction commercial modules [30]. The world record efficiency for c-Si solar cells is currently 26.33% on a heterojunction with intrinsic layer (HIT) interdigitated back contact (IBC) solar cell made by Kaneka Corporation. This cell is an example of the individually optimized characteristics necessary for solar cell efficiencies above the 25% level and approaching the fundamental limitations of c-Si solar cell efficiencies. In order to attain this efficiency, excellent surface passivation, as evidenced from the high V_{oc} (743.8 mV), is combined with excellent light trapping (42.25 mA/cm^2). While this cell was probably made without the use of nanostructures, advanced light management with nanostructures make it possible to further enhance these characteristics of the cell and beyond the 25.6% cell efficiency.

Conventional light trapping for c-Si solar cells, namely, chemical texturing and application of antireflection coatings, has already led to effective light trapping performance, achieving short-circuit current greater than 42 mA/cm^2 on the unshadowed (unmetallized) portion of industrially manufactured cells. However, conventional texture has a number of limitations to realizing inexpensive solar device at much higher efficiency.

The typical feature size of chemical texturing is in the range of 3–10 μm [31,32]. On conventional c-Si solar cells, with a thickness in the range 140–180 of μm, the pyramidal light-trapping texture, coated with an 80 nm thick Si_3N_4 antireflection layer, is not limiting. Despite providing excellent antireflection and light trapping properties for a 180 μm thick cell, this scheme cannot be used for thinner cells in the micrometer range, due to the large feature size. Surface Mie nanoscatterers are an ideal candidate to substitute the micrometer-sized pyramidal texture on thinner cells. In fact, due to the high index of c-Si (~3.5 at 1100 nm), the strong scattering of light mediated by the Mie resonances in the nanoparticles can be used to preferentially couple light into the c-Si. For example, it has been shown that it is possible to make 10 μm thick c-Si cells with 20% efficiency by using a Si Mie coating [33]. Another potential limitation of conventional chemical texturing is that the process inherently relies on surface defects to initiate etching and increases the surface area: a dependence that results in surfaces that are more recombination active and more difficult to passivate. Finally, chemical texture works very well on monocrystalline Si solar cells, but is less effective on less expensive multicrystalline Si wafers that now make up a large portion of the market. Mie resonant nanoparticles could offer solutions for increasing the current on these wafers, as well as on other nonstandard substrates that are now entering the market.

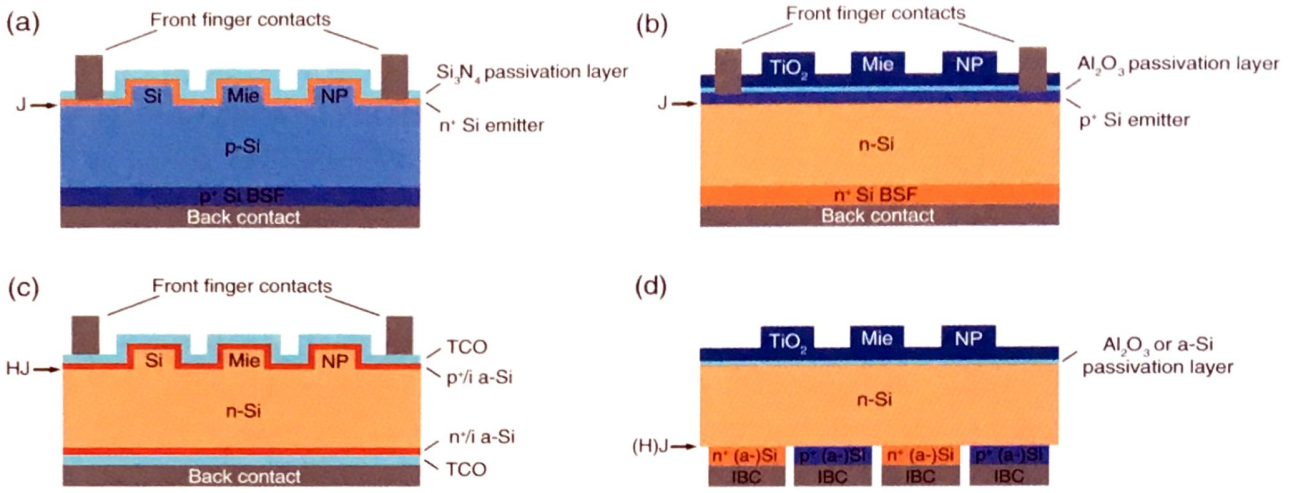

Figure 7.1 Four crystalline Si solar cell designs that can benefit from a Si and TiO_2 nanoparticle coating. (a) Si Mie coating applied to a standard p-type Si-based solar cell with diffused front junction. (b) TiO_2 Mie coating on an n-type Si-based solar cell with diffused front junction. (c) a-Si:H/c-Si heterojunction with intrinsic layer (HIT) solar cell with a Si Mie coating. (d) Interdigitated back contact (IBC) homojunction (or heterojunction) solar cell with a TiO_2 Mie coating.

7.2.1
Integration of Mie Coatings on c-Si Cell Architectures

Here we present and discuss the integration of surface Mie nanoscatterers to four different c-Si solar cell architectures.

Figure 7.1 shows the schematics of four existing c-Si solar cell designs on which Si [8] or TiO_2 [11] Mie coatings can be integrated. Figure 7.1a shows the most widely used configuration in commercial c-Si cells. In this configuration, a p-type c-Si substrate is used, in combination with a highly doped p-type Si layer at the back acting as a back surface field (BSF) to repel minority carriers, and a metal back contact (usually Al). The Si Mie coating can be integrated (by reactive ion etching) in the front surface of the p-type layer. A highly doped n-type Si layer at the front, conformal to the Si NPs, can then be introduced by phosphorus diffusion to form a shallow junction. A Si_3N_4 layer with thickness of 50 nm is finally applied to passivate the surface and serve as an antireflection coating [34]. Screen-printed metallic (Ag) finger contacts can be used at the front. The advantages of this configuration are the excellent antireflection and light trapping properties provided by the Si Mie coating, compared to a standard texture [8], and the absence of parasitic losses in the Mie scatterers, as they are part of the active material. However, this geometry presents some drawbacks. It has been shown that the reactive ion etching (RIE) used to fabricate the Si nanopillars creates additional surface area and near-surface defects in the Si, thus increasing carrier recombination [11]. A standard Al_2O_3 passivation layer is ineffective to fully passivate the Si Mie scatterer surface. A different RIE process,

based on chemical etching of Si rather than on physical etching, must be used to yield Si surfaces that can be passivated with Al_2O_3 [35]. A second drawback of the geometry shown in Figure 7.1a is that the Mie resonances in the Si NPs enhance the absorption of light in the NPs, that is, close to the high-recombination region of the highly doped emitter. Finally, the metal contacts are highly recombination active and cause shadowing of light, thus limiting the efficiency of the cell.

Figure 7.1b shows the schematic of a solar cell based on an n-type Si wafer. These wafers present two important advantages with respect to p-type wafers for achieving higher efficiencies: first, they do not suffer from light-induced degradation due to boron–oxygen centers; second, they are less sensitive to interstitial metal impurities [36,37]. The cell configuration is similar to that of Figure 7.1a. A diffused heavily doped p-type layer is used in this case to form the junction. For p-type Si, Al_2O_3 yields excellent field passivation due to the built-in negative charge [38]. This cell configuration can therefore take advantage of the TiO_2/Al_2O_3 antireflection and passivation coating [11]. As in the case of Figure 7.1a, metallic finger contacts can be applied at the front. The advantages of this configuration are the excellent antireflection and passivation properties provided by the TiO_2 Mie scatterers and by the thin Al_2O_3 layer, respectively, the low parasitic losses in the visible and infrared spectral range [11], and the good light trapping properties [33]. One drawback, as for the cell in Figure 7.1a, is that the TiO_2 Mie scatterers slightly enhance light absorption in the high-recombination p-type emitter at the front, due to the fact that the geometrical Mie resonance overlaps with this region. Shadowing from the front contact also limits the overall cell efficiency.

Figure 7.1c shows an application of the Si Mie coating to HIT thin-layer c-Si solar cells. These cells are based on an n-type c-Si wafer. An n-doped hydrogenated amorphous Si (a-Si:H) layer is used at the back, as a wider bandgap layer to repel the minority carriers from recombining at the back surface. Similarly, a p-doped a-Si:H layer is used at the front, forming the solar cell junction. An intrinsic a-Si:H intermediate layer is used on both sides, below the doped layers, to reduce the surface state density, thus improving surface passivation [39]. Transparent conductive oxides (TCOs) such as indium tin oxide (ITO) are then used in combination with metal grid contacts to extract the carriers from the cell. The separation of the active layer from the highly recombination-active metal contacts provides a high open-circuit voltage and therefore a higher efficiency [39]. The Si Mie coating may be integrated in the HIT cell, as shown in Figure 7.1c. By making an ultrathin junction conformal to the Si NPs, photocarriers generated inside the c-Si NPs can be efficiently extracted from the cell. The HIT Si cell can thus take full advantage of the antireflection and light trapping properties of the Si Mie coating. Possible drawbacks of this configuration are the fact that it may be difficult to achieve good passivation of the Si Mie scatterer surface. Moreover, the HIT design suffers from increased parasitic losses in the front TCO and a-Si:H layers. As the two designs above, front contact shadowing also limits the cell performance.

Figure 7.1d is a schematic of an interdigitated back contact back-junction c-Si solar cell. As the name indicates, this cell is characterized by the fact that all metallic contacts and the junction are at the backside of the cell. The junction can be either a c-Si homojunction or an a-Si:H heterojunction similar to the one described in Figure 7.1c. The back of the cell alternates highly p-doped Si regions (forming the junction) with highly n-doped regions (forming a BSF), in an interdigitated finger configuration. The front of the cell is usually textured but can also be made totally flat, thus reducing surface recombination. For a flat front-side configuration, a TiO_2 Mie coating made on top of a thin passivation layer is an ideal antireflection and light trapping scheme. Al_2O_3 can be used as a passivation layer also for n-type Si, as it creates an inversion layer near the surface where holes become majority carriers [38]. Alternatively, an intrinsic a-Si:H layer can be used as a passivation layer. The main advantage of this configuration is the absence of any front-shadowing element. The front can be fully patterned with a TiO_2 Mie coating, which is an excellent ARC and has no parasitic losses in the spectral range above 400 nm [11]. Another advantage with respect to the previous geometries is that the enhanced light absorption in proximity of the NPs due to the overlap of Mie resonances with the substrate is decoupled from the highly doped region of the emitter (which is at the back). Overall, the configuration in Figure 7.1d takes full advantage of the strong scattering properties of the Mie coating, without any major drawback.

7.2.2
Nanostructures for Improved Surface Passivation

Most of the discussion up to here has been focused on the use of nanostructures for enhanced light trapping or increased short-circuit current. In the case of c-Si, conventional light trapping methods of surface texture and antireflection coatings offer very efficient light trapping for standard thickness and even very thin Si substrates (>100 μm). Nanostructures, as discussed above, do not necessarily offer better light trapping than the methods of conventional texturing [40]. One of the unique features of nanostructures as a replacement for texture or conventional light trapping methods is that they can be applied on flat surfaces and even made from a different materials than the underlying active material, as suggested in the TiO_2 structures in Figure 7.1b and d [41]. Flat surfaces on absorber or active layers offer a number of possible advantages in optimizing electrical behavior of solar cells, especially in looking at the next generation of high efficiency solar cell architectures. These advantages include improved surface passivation and reduced carrier recombination, less recombination-active junction area, thinner substrates, and less parasitic absorption by surface layers due to decreased effective thickness. All of these benefits can be exploited through the use of nanostructures that replace the texture for light trapping.

7.2.2.1 Surface Passivation

In cells with conventional light trapping, like random or inverted pyramids, the surface of the actual semiconductor is etched and the area is increased. However, the same surface is also in proximity to the location where carriers are created and collected. This surface is an area of high recombination within the device due to the doping, interface properties, and surface defects. In order to overcome the effect of these surface properties, surface passivation or reducing the rate of recombination at the surface of devices is a main limitation of increasing cell efficiency [42,43]. Today, this requires passivation of a textured surface. Nanostructures for photovoltaic devices offer an opportunity to decouple light trapping from surface recombination. Nanostructures can be patterned in a layer or material separate that is electrically isolated from the electrically active area of the semiconductor, minimizing the surface area and defect density. In this case, the improvement in surface passivation could be at a minimum a factor of 1.6 times better due to the inherent geometry of a pyramidal textured surface for high-performance surface passivation schemes [42]. For many passivation technologies, recombination on polished surfaces has been shown to be 10–100 times better than on textured surfaces [43].

7.2.2.2 Thin Devices

Surface recombination also plays a more significant role in very thin devices. When the diffusion length of the carriers is multiple times longer than the thickness of the cell, the lifetime of minority carriers will be dominated by surface recombination. Advances in surface passivation, development of new materials, and increased interest in heterojunctions and passivated contact-type solar cells have led to surface recombination velocities less than 10 cm/s on textured wafers [43]. This also creates an opportunity for realizing improved efficiency with thinner wafers. Assuming very low or no surface recombination, excellent light trapping, and high lifetime material, the potential V_{oc} of a cell will increase as the thickness decreases. Figure 7.2 shows a PC1D [44] simulation of a silicon device with 3 ms bulk lifetime and 4 cm/s surface recombination velocity (J_0 model) as a function of thickness, for both a textured and an untextured cell. We assume that for the untextured cell, the short-circuit current is similar to that of the textured cell, as seen in experiments and simulations for standard thickness Si substrates. The improvement in open-circuit voltage in this case is on the order of 13 mV for all thicknesses [42].

7.2.3 Properties of Nanostructured Coatings for Si Solar Cells

Table 7.1 compares the performance of different dielectric (Mie) or metallic (plasmonic) resonant nanostructures with respect to several properties of Si solar cell. The results are based on published literature (see references indicated in square brackets). Three main kinds of resonant nanoscatterers have been

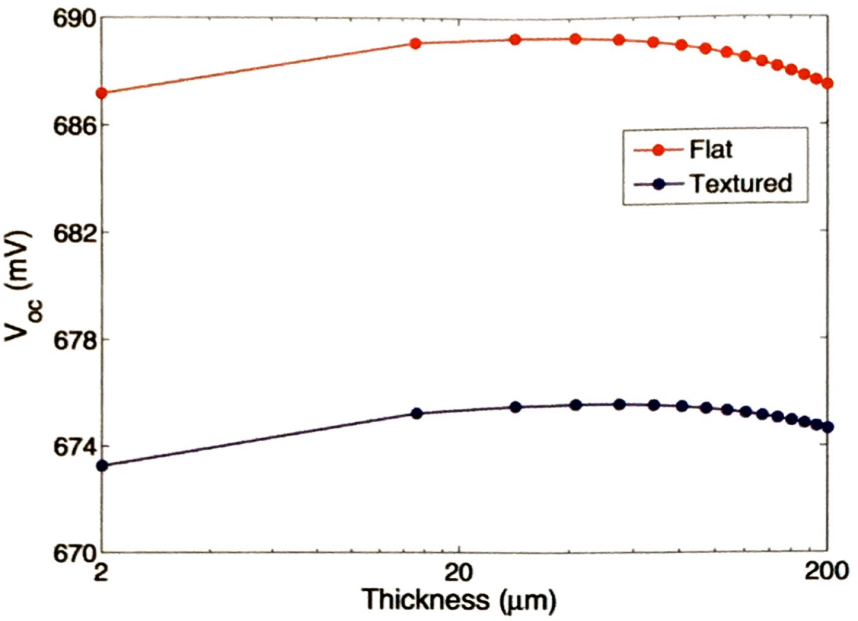

Figure 7.2 Simulated (PC1D) V_{oc} as a function of thickness for a textured and an untextured cell assuming equal current at each thickness and 3 ms lifetime substrate with 4 cm/s surface recombination velocity.

considered: Si, TiO_2 (Mie), and Ag (plasmonic) NPs. The first column of the table lists several properties that are key to achieving high efficiency for c-Si solar cells. Green color is used to indicate good or excellent results, orange indicates that there are some limitations, and red means that the NP coating is unsuited for that purpose or solar cell design.

Table 7.1 Summary of the effect for Si, TiO_2, and Ag nanoparticle coatings for several properties of solar cell designs that are key to achieving high efficiency.

Solar cell properties	Si Mie coating	TiO_2 Mie coating	Ag plasmonic coating
Antireflection	Excellent ($R = 1.3\%$) [8]	Excellent ($R = 1.6\%$) [11]	Fair ($R \sim 7\%$) [7]
Light trapping (in 1–100 μm cell)	Excellent (21.5% @20 μm) [33]	Good (19.8% @20 μm) [33]	Fair based on Ref. [7,44][a)]
Surface passivation	Difficult ($\tau = 10$ μs) [11]	Excellent ($\tau = 4$ ms) [11]	Excellent based on Ref. [11][b)]
Parasitic losses	None (integrated) [8]	Low (only <400 nm) [11]	High (>5%) [44]
AR effect with EVA encapsulation	Excellent ($R < 2.1\%$) [40]	Very good ($R < 4.2\%$) [40]	Poor (>standard ARC) [40]

Notes:

a) Because of parasitic losses in the metal.

b) Because the Ag plasmonic coating can be applied to a flat, passivated solar cell surface, similar to the TiO_2 Mie coating.

Table 7.1 clearly shows that overall the TiO_2 Mie coating offers the best opportunities for application to Si solar cells, compared to the Si and Ag NP coatings. The TiO_2 Mie coating provides excellent antireflection and passivation properties for Si solar cells; it also provides very good light trapping properties; it can be used in combination with EVA encapsulation; the parasitic losses are small and limited to the spectral range below 400 nm [11].

The Si Mie coating can also be effectively applied to a variety of cell configurations and for different purposes. The AR and light trapping properties for c-Si cells are better than those of the TiO_2, and there are no parasitic losses as the coating is part of the active layer. However, the main drawback of the Si Mie coating is the difficulty in achieving a good surface passivation. Furthermore, absorption in the Si NPs becomes an issue when they are applied to GaAs solar cells and polymer solar cells (not shown in table).

The plasmonic coating is strongly limited in all applications by substantial parasitic losses due to ohmic damping. A fairly good AR effect can be achieved for Si solar cells. However, the high sensitivity of the plasmon-mediated scattering to changes in the local optical environment makes the plasmonic coating impractical in combination with EVA encapsulation [40]. The light trapping properties of plasmonic NPs for Si solar cells were not studied in this work. However, based on the studies of AR effect and ohmic losses carried out in Refs [7,44], only a limited light trapping effect is expected. The effect of Ag NPs on surface passivation was also not investigated in this work. Note that the plasmonic coating can be made on top of a Si_3N_4 dielectric layer, which is usually employed also for surface passivation in c-Si solar cells. We thus expect the plasmonic coating to be easily integrated with a passivation layer, similar to the TiO_2 Mie coating. The Si_3N_4 spacer layer can also be substituted by or integrated with an Al_2O_3 passivation layer for better surface passivation, as the two materials have similar refractive index ($n = \sim 2$).

7.3 Nanostructured Coatings for Thin-Film Solar Cells

Solar cells based on c-Si are not the only PV technology that can benefit from the use of nanostructures. In this section we analyze two thin-film PV technologies that can take advantage of resonant nanostructures: high-efficiency GaAs solar cells and low-cost polymer solar cells.

7.3.1 Application to High-Efficiency GaAs Solar Cells

GaAs solar cells currently hold the world record efficiency for single-junction cells, both on cell and on module level [30]. Due to close-to-unity quantum efficiency, open-circuit voltages up to 1.1 eV and efficiencies up to 28.8% have been demonstrated. GaAs solar cells use no light trapping scheme as the active layer is

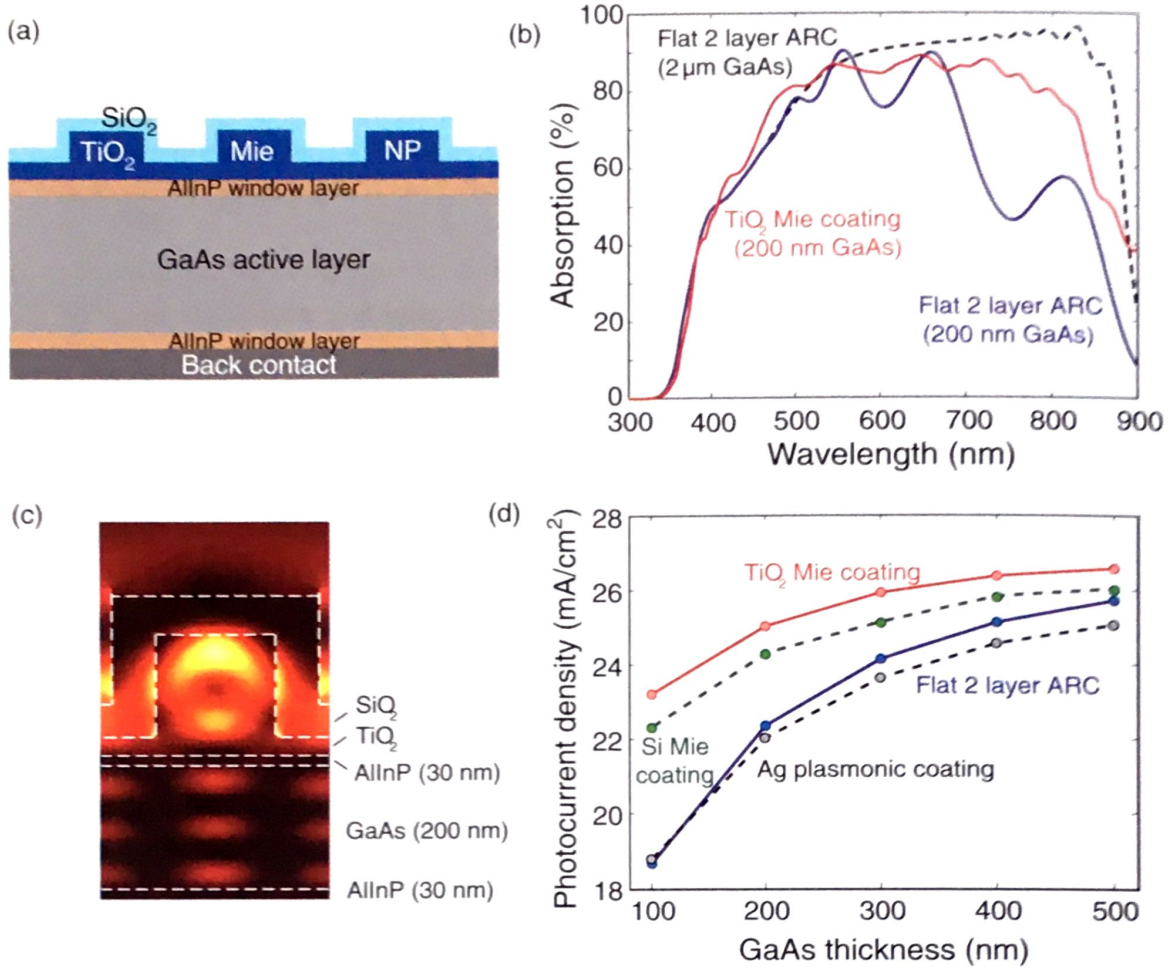

Figure 7.3 Application of Mie and plasmonic coatings to high-efficiency GaAs solar cells. (a) Schematic of a GaAs solar cell with the TiO_2 Mie coating. (b) Simulated absorption spectra for a 2 μm thick GaAs solar cell with double-layer ARC (dashed black line), a 200 nm thick GaAs cell with double-layer ARC (solid blue line), and for a 200 nm thick GaAs cell with TiO_2 Mie ARC (solid red line). (c) Electric field intensity distribution (color scale) in a vertical cross section of the GaAs cell with the TiO_2 Mie coating, for a wavelength of 800 nm. (d) Simulated photocurrent density as a function of solar cell thickness for a GaAs solar cell with a standard double-layer ARC (solid blue), a TiO_2 Mie coating (solid red), a Si Mie coating (dashed green), and a Ag plasmonic coating (dashed black).

thick enough to absorb nearly all light with wavelength up to the bandgap. Surface Mie scatterers can be used in this case to reduce the active layer thickness, and thus reduce the overall fabrication costs of the cell, while maintaining the same absorption of light.

Figure 7.3a shows a schematic of a GaAs cell with a TiO_2 Mie coating. The cell comprises an AlInP/GaAs/AlInP layer stack, a metal back contact, and a TiO_2 NP array coated with a thin SiO_2 layer at the front. GaAs is used as the active layer of the cell, while AlInP is used for the two window layers. Due to the wider bandgap with respect to GaAs, the AlInP layers repel the minority carriers from the surface, thus avoiding surface recombination.

Figure 7.3b shows the simulated absorption spectra for a 2 μm thick GaAs solar cell with a flat double-layer ARC (dashed black line), a 200 nm thick GaAs cell with a flat double-layer ARC (solid blue line), and for a 200 nm thick GaAs cell with a TiO_2 Mie ARC (solid red line). TiO_2 cylinders with a height of 100 nm and diameter of 350 nm are used in a square array with pitch of 700 nm. The 2 μm thick cell with a flat double-layer ARC absorbs almost all the light in the spectral range 500–850 nm. The absorption drops below 500 nm due to parasitic losses in the TiO_2 and AlInP window layer. The drop in absorption at 870 nm corresponds to the bandgap of GaAs. From simulations, it follows that the losses due to reflection or incomplete light trapping amount to less than 2%. The absorption of a 200 nm thick GaAs solar cell (solid blue) in the spectral range below 500 nm is similar to that of a 2 μm thick cell, and it is limited by parasitic absorption in the window layer. However, for wavelengths above 600 nm, the absorption drops due to incomplete light trapping. The oscillations in the absorption spectrum are due to Fabry–Pérot interference in the thin layer stack. Applying the TiO_2 Mie coating on the 200 nm thick cell strongly enhances light absorption in the visible and near-infrared spectral range (solid red line). A fourfold absorption enhancement is observed for wavelengths close to the GaAs bandgap. The absorption enhancement is due to the coupling of light to waveguide modes in the thin GaAs layer through scattering by leaky Mie resonances in the TiO_2 NPs. Figure 7.3c shows an example of a waveguide mode in the GaAs layer. The figure shows the electric field intensity distribution (color scale) in a vertical cross section of a GaAs cell with the TiO_2 Mie coating, for a wavelength of 800 nm. A periodic electric field pattern is observed in the GaAs layer, corresponding to a waveguide mode in the layer. A clear magnetic dipole Mie resonance is visible inside the TiO_2 NP.

The absorption spectra shown in Figure 7.3b can be used to calculate the fraction of photons absorbed in the GaAs layer and the total generated photocurrent, assuming 100% photon-to-carrier conversion efficiency. Figure 7.3d shows the photocurrent density as a function of GaAs layer thickness, for a cell with a flat double-layer ARC (solid blue line) and a cell with the TiO_2 Mie coating (solid red). As can be seen, the photocurrent is strongly enhanced for all thicknesses due to the TiO_2 Mie scatterers. The photocurrent enhancement is more significant for thinner cells where light trapping is more relevant. For a 100 nm thick cell, the photocurrent is enhanced by 30% due to the TiO_2 Mie coating.

For thicker cells, the photocurrent of the cells with a flat coating and with the TiO_2 Mie coating converge to the same value, corresponding to full light absorption. Figure 7.3d shows that a 200 nm thick cell with TiO_2 Mie coating generates nearly as much photocurrent as a 500 nm thick cell. Therefore, the TiO_2 Mie coating allows a significant reduction of material usage, and thus costs, while maintaining similar performance. The graph also shows, for comparison, the simulated photocurrent obtained with a Si Mie coating (dashed green line) and a plasmonic Ag NP coating (dashed black). In both cases, a lower photocurrent with respect to that of a TiO_2 Mie coating is

observed for all thicknesses, due to parasitic losses in the NPs. For the case of Ag NPs, the parasitic losses are so large that the cell is outperformed by a flat cell with a double-layer ARC.

7.3.2 Nanostructured Coatings for Organic Solar Cells

For Si and GaAs solar cells, the plasmon-mediated or Mie-mediated scattering of light occurs preferentially toward the high-index substrate, mainly due to the higher density of optical states. This yields ultralow reflectivities and strong light trapping properties. However, when lower index substrates are considered, for example, organic solar cells, the scattering is usually more isotropic. Therefore, alternative routes must be investigated. It has been shown that plasmonic nanoparticles embedded in a polymer solar cell enhance light absorption in the polymer due to the concentration of light in the near field of the metal NP [44]. This absorption enhancement however comes at the expense of strong parasitic losses in the metal NP due to ohmic damping. In the following, an alternative concept to direct light into low-index polymer solar cells is presented, based on lossless (or low-loss) dielectric nanoparticles.

Dielectric NPs have electric and magnetic Mie modes [45,46]. The magnetic resonances stem from displacement currents excited by the incident light inside the NP. The interference of magnetic and electric modes inside the high-index dielectric NPs affects their scattering behavior [47]. It can be shown that in dielectric NPs with large refractive index ($n \sim 3$–4), backscattering of light can be strongly suppressed if the electric and magnetic dipoles oscillate in phase [48]. This phenomenon is similar to the scattering behavior of a hypothetical $\varepsilon = \mu \neq 1$ particle predicted by Kerker *et al.* in 1982 [49]. In the following, the suppressed backscattering by high-index dielectric NPs will be referred to as "Kerker scattering." Recently, experimental demonstration of "Kerker scattering" has been shown for Si [50] and GaAs [49] NPs on glass. The "Kerker scattering" can be used to direct light into a low-index substrate, and thus it can be used to enhance absorption in polymer solar cells.

Figure 7.4a shows a schematic of a typical organic solar cell [51]. The active layer is a mixture of poly(3-hexylthiophene-2,5-diyl) (P3HT) and phenyl-C_{61}-butyric acid methyl ester (PCBM). The index of this polymer blend is $n \sim 1.5$. A TiO_2 ($n \sim 2.3$) layer at the back acts as an electron transport layer (ETL), while a poly(3,4-ethylenedioxythiophene) and poly(styrenesulfonate) polymer blend (PEDOT:PSS, $n \sim 1.6$) acts as a hole transport layer (HTL). The back and front contacts are metal and TCO, respectively. A high-index dielectric NP is placed on top of the TCO, in order to exploit the enhanced forward scattering of light due to Kerker scattering.

In order to study this effect, the case of a spherical dielectric NP on top of a glass ($n = 1.46$) substrate is considered. A high-index NP needs to be chosen in order to effectively suppress the backscattering. Si, GaAs, or Ge are good

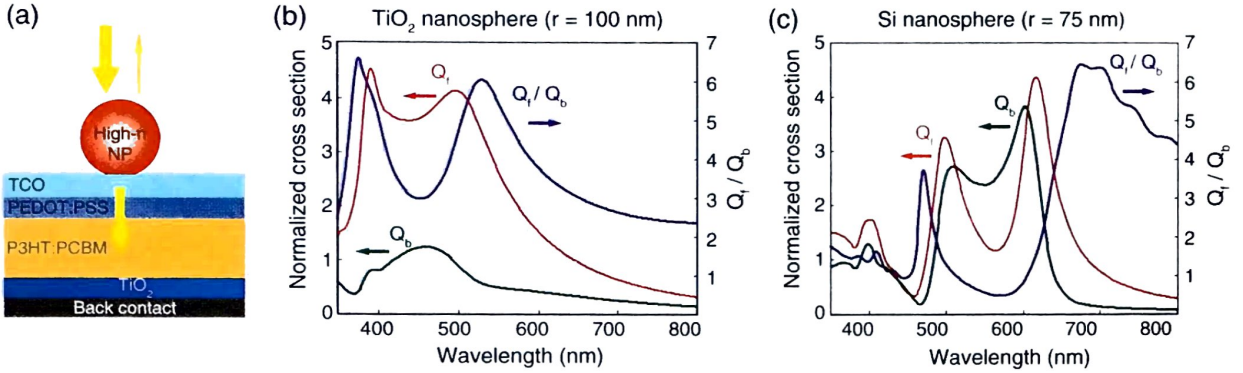

Figure 7.4 A concept based on the "Kerker scattering" of high-index dielectric NP for improving the absorption of light in low-index polymer solar cells. (a) Schematic of a typical polymer solar cell with a dielectric nanoscatterer at the front. (b) Forward (red) and backward (green) scattering cross sections, normalized to the NP area (left axis), for a 200 nm diameter TiO_2 NP on glass. The forward-to-backward scattering ratio is also shown (blue, right axis). (c) Same plot as in part (b), for a 150 nm diameter Si NP on glass.

materials to achieve this. However, GaAs and Ge have high absorption in the visible spectral range, and thus less interesting for achieving large forward scattering. On the other hand, TiO_2 has a lower index ($n \sim 2.3$), but is lossless in the visible range.

Figure 7.4b shows the simulated forward (red) and backward (green) scattering cross section (SCS) spectra for a 200 nm diameter TiO_2 sphere on glass. The SCS spectra are normalized to the geometrical cross section of the NP, and they refer to the graph left axis. The forward SCS shows two resonances: a magnetic dipole resonance at ~500 nm and an electric dipole resonance at ~400 nm. At both resonances, the forward SCS is more than four times larger than the geometrical area of the NP. The graph also shows the forward-to-backward SCS ratio (blue line, axis on the right). As can be seen, the forward SCS dominates the backward SCS over the entire spectral range of 350–800 nm. The forward SCS enhancement with respect to the backward SCS is larger than 2 in the entire spectral range considered. The ratio peaks at wavelengths below the electric dipole resonance and above the magnetic dipole resonance. At the peak, the forward-to-backward SCS ratio is larger than 6.

Figure 7.4c shows the simulated forward (red) and backward (green) normalized SCS spectra (left axis) for a 75 nm radius Si sphere on glass. The forward-to-backward SCS ratio is also shown (blue, right axis). Similar to the case of a TiO_2 particle, the graph shows that the forward scattering is enhanced for wavelengths below the electric dipole resonance and above the magnetic dipole resonance. In this case, it can be noted that for wavelengths in-between the two resonances, the backward SCS is larger than the forward SCS. Nonetheless, in the broad spectral range of 600–800 nm, the forward scattering is strongly enhanced, with a forward-to-backward scattering ratio exceeding 4.

The strong broadband enhancement of the forward scattering may be used to provide an AR coating for low-index polymer solar cells. Changing the NP size gives some tunability of the spectral range over which the forward scattering is enhanced.

7.4 Other PV Applications of Resonant Nanostructures

This chapter has focused mostly on nanostructured coatings for solar cells, in which dielectric and metallic nanoparticles are placed at the front side of the solar cell. There are, however, several other application of nanostructures in different configurations that are also beneficial for solar applications. Here some examples are briefly discussed.

As already mentioned, plasmonic nanoparticles are limited by parasitic ohmic absorption. However, they also present the advantage of being made of conductive metals. Recent studies have shown that metal nanowire networks combine unique transparency and conductivity properties. Using Ag nanowire networks, light transmission above 90% and sheet resistance below 20 Ω/sq have been achieved [12]. Ag nanowire networks can thus be used as a transparent conductive electrode as an alternative to standard transparent conductive oxides (TCOs). These nanostructures applied to standard HIT solar cells allow achieving better FF values than the industrial ITO.

In addition to front-side coating made of nanoparticles or nanowires, also rear-side nanostructures have shown promising results for application to thin-film solar cells. Many recent studies have shown that both plasmonic and dielectric nanostructures at the rear side of thin-film a-Si solar cell enhance photocurrent generation due to coupling to waveguide modes in the thin layer [52,53]. Also other thin-film solar technologies such as CIGS solar cells can benefit from nanostructures at the rear side [54]. Distributed Bragg reflectors alternating layers of different dielectric material with nanometer thicknesses have also been used to improve the rear-side reflectivity of c-Si solar cells [55].

Finally, nanostructures are beneficial not only for application on solar cells but also on module level. The reflectivity of module glass is a well-known problem for photovoltaic application. For light under normal incidence, standard PV glass reflects more than 4% of the incoming light. The reflectivity is even higher for larger angles of incidence. In recent studies, nanostructured coatings for glass have been developed that allow reducing reflectivity significantly for all angles of incidence [56]. The nanostructured coatings can be readily fabricated on large scale by nanoimprint techniques such as Substrate Conformal Imprint Lithography (SCIL) [57]. Developed in recent years, this technique allows controlling the nanoparticle geometry down to the nanometer scale and reproducing nanoparticle patterns with high fidelity over a large scale. It opens new perspectives to realize nanostructured designs at the square kilometer level. By using SCIL, a nanostructured coating for glass has been realized with integrated reflectivity of only 0.9%, which showed a relative increase of the power output of a solar minimodule by 2.8% (see Figure 7.5).

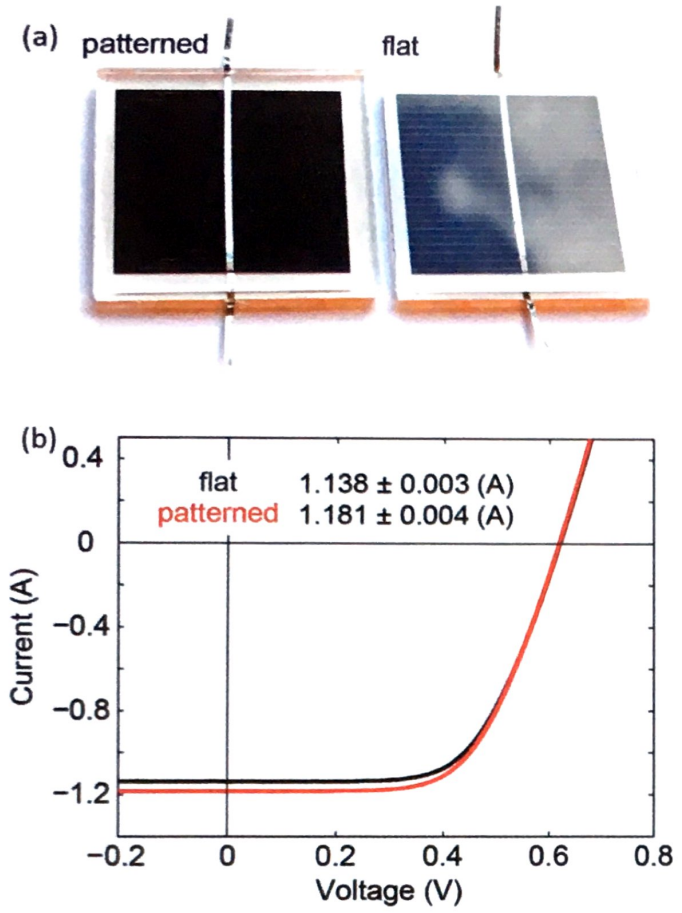

Figure 7.5 Nanostructured coating for module glass. (a) Photograph of a mini-module with nanostructured coating (left) and without coating (right). (b) Current–voltage measurement of the mini-modules showing a 2.8% relative increase in power output due to the nanostructured coating. (Reproduced with permission from Ref. [56].)

7.5 Summary

The beneficial effects of using nanostructured coatings on different solar cell technologies have been presented. From the optical point of view, nanostructures offer the possibility to strongly enhance the absorption of light into the active layer (light trapping) due to the strong interaction of the resonant nanoparticles with light. This results in enhanced photocurrent generation in both c-Si solar cell and other thin-film technologies, such as GaAs, CIGS, or organic solar cells. Among the different materials that can be used for the nanostructured coating, dielectrics with high refractive index (such as Si or TiO_2) are the most suited due to the strong light scattering behavior and the small parasitic optical losses. Metal nanoparticles, while showing similar scattering properties, are less suited due to the presence of significant parasitic losses.

Besides the enhanced optical effect, nanostructures also offer the possibility to enable new solar cell designs that are beneficial in terms of reduced carrier

recombination. For example, TiO_2 nanostructures can be readily integrated on c-Si solar cells with flat surfaces, where the surface recombination is minimized. A flat surface allows a V_{oc} gain for c-Si solar cells of more than 10 mV with respect to standard textured surfaces.

Furthermore, carrier collection from the active material of the solar cells can also benefit from the front- and rear-side metal nanostructures. Silver nanowire grids, for example, allow effective carrier transport and light transparency properties and are thus a valid replacement of standard transparent conductive layers such as ITO.

Overall, the novel designs based on resonant nanostructures uniquely allow decoupling light trapping architectures from surface passivation and carrier collection schemes, thus enabling a separate optimization of each of these aspects. Furthermore, they can also be applied on module level to improve the antireflection properties of glass modules. All the nanostructure designs presented in this chapter can be realized at the square kilometer level in a practical way by using novel nanoimprint techniques such as SCIL.

References

1 Atwater, H.A. and Polman, A. (2010) Plasmonics for improved photovoltaic devices. *Nat. Mater.*, **9**, 205–213.

2 Polman, A. and Atwater, H.A. (2012) Photonic design principles for ultrahigh-efficiency photovoltaics. *Nat. Mater.*, **11**, 174–177.

3 Brongersma, M., Cui, Y., and Fan, S. (2014) Light management for photovoltaics using high-index nanostructures. *Nat. Mater.*, **13**, 451–460.

4 Kreibig, U. and Vollmer, M. (1995) *Optical Properties of Metal Clusters*, Springer.

5 Bohren, C.F. and Huffman, D.R. (2008) *Absorption and Scattering of Light by Small Particles*, John Wiley & Sons, Inc., New York.

6 Mie, G. (1908) Beitrage zur Optik truber Medien, speziell kolloidaler Metallosungen. *Ann. Phys. (Berlin)*, **330**, 377–445.

7 Spinelli, P., Hebbink, M., de Waele, R., Black, L., Lenzmann, F., and Polman, A. (2011) Optical impedance matching using coupled plasmonic nanoparticle arrays. *Nano Lett.*, **11**, 1760–1765.

8 Spinelli, P., Verschuuren, M.A., and Polman, A. (2012) Broadband omnidirectional antireflection coating using subwavelength surface Mie resonators. *Nat. Commun.*, **3**, 692.

9 Catchpole, K.R. and Polman, A. (2008) Design principle for particle plasmon enhanced solar cells. *Appl. Phys. Lett.*, **93**, 191113.

10 Kippenberg, T.J., Tchebotareva, A.L., Kalkman, J., and Polman, A. (2009) Purcell-factor-enhanced scattering from Si nanocrystals in an optical microcavity. *Phys. Rev. Lett.*, **103**, 027406.

11 Spinelli, P., Macco, B., Verschuuren, M.A., Kessels, W.M.M., and Polman, A. (2013) Al_2O_3/TiO_2 nano-pattern antireflection coating with ultralow surface recombination. *Appl. Phys. Lett.*, **102**, 233902.

12 van de Groep, J., Spinelli, P., and Polman, A. (2012) Transparent conducting silver nanowire networks. *Nano Lett.*, **12**, 3138.

13 Mokkapati, S., Beck, F.J., Catchpole, K.R., and Polman, A. (2009) Designing periodic arrays of metal nanoparticles for light-trapping applications in solar cells. *Appl. Phys. Lett.*, **95**, 053115.

14 Derkacs, D., Lim, S.H., Matheu, P., Mar, W., and Yu, E.T. (2006) Improved performance of amorphous silicon solar cells via scattering from surface plasmon

polaritons in nearby metallic nanoparticles. *Appl. Phys. Lett.*, **89**, 093103.

15 Pillai, S., Catchpole, K.R., Trupke, T., and Green, M.A. (2007) Surface plasmon enhanced silicon solar cells. *J. Appl. Phys.*, **101**, 093105.

16 Tvingstedt, K., Person, N.K., Inganas., O., Rahachou, A., and Zoloulenko, I.V. (2007) Surface plasmon increase absorption in polymer photovoltaic cells. *Appl. Phys. Lett.*, **91**, 113514.

17 Haug, F.J., Söderström, T., Cubero, O., Terrazzoni-Daudrix, V., and Ballif, C. (2008) Plasmonic absorption in textured silver back reflectors of thin film solar cells. *J. Appl. Phys.*, **104**, 064509.

18 Franken, R.H., Stolk, R.L., Li, H., van der Werf, C.H.M., Rath, J.K., and Schropp, R.E.I. (2007) Understanding light trapping by light-scattering textured back electrodes in thin-film n-i-p silicon solar cells. *J. Appl. Phys.*, **014503**, 102.

19 Saeta, P.N., Ferry, V.E., Pacifici, D., Munday, J.N., and Atwater, H.A. (2009) How much can guided modes enhance absorption in thin film solar cells? *Opt. Express*, **17**, 20975–20990.

20 Ferry, V.E., Verschuuren, M.A., Li, H.B.T., Schropp, R.E.I., Atwater, H.A., and Polman, A. (2009) Improved red-response in thin film a-Si:H solar cells with soft-imprinted plasmonic back reflectors. *Appl. Phys. Lett.*, **95**, 183503.

21 Ferry, V.E., Verschuuren, M.A., van Lare, M., Schropp, R.E.I., Atwater, H.A., and Polman, A. (2011) Optimized spatial correlations for broadband light trapping nanopatterns in high efficiency ultrathin film a-Si:H solar cells. *Nano Lett.*, **11**, 4239–4245.

22 Rand, B.P., Peumans, P., and Forrest, S.R. (2004) Long-range absorption enhancement in organic tandem thin-film solar cells containing silver nanoclusters. *J. Appl. Phys.*, **96**, 7519–7526.

23 Morfa, A.J., Rowlen, K.L., Reilly, T.H., III, Romero, M.J., and van de Lagemaat, J. (2008) Plasmon-enhanced solar energy conversion in organic bulk heterojunction photovoltaics. *Appl. Phys. Lett.*, **92**, 013504.

24 Lindquist, N.C., Luhman, W.A., Oh, S.H., and Holmes, R.J. (2008) Plasmonic nanocavity arrays for enhanced efficiency in organic photovoltaic cells. *Appl. Phys. Lett.*, **93**, 123308.

25 Hagglund, C., Zach, M., and Kasemo, B. (2008) Enhanced charge carrier generation in dye sensitized solar cells by nanoparticle plasmons. *Appl. Phys. Lett.*, **92**, 013113.

26 Standridge, S.D., Schatz, G.C., and Hupp, J.T. (2009) Distance dependence of plasmon-enhanced photocurrent in dye-sensitized solar cells. *J. Am. Chem. Soc.*, **131**, 8407.

27 Tanabe, K. (2009) A review of ultrahigh efficiency III–V semiconductor compound solar cells: multijunction tandem, lower dimensional, photonic up/down conversion and plasmonic nanometallic structures. *Energies*, **2** (3), 504–530.

28 Alu, A. and Engheta, N. (2008) Multifrequency optical invisibility cloak with layered plasmonic shells. *Phys. Rev. Lett.*, **100**, 113901.

29 Jager-Waldau, A. (2015) PV Status Report 2015. Technical report, Joint Research Center.

30 Green, M.A., Emery, K., Hishikawa, Y., Warta, W., and Dunlop, E.D. (2016) Solar cell efficiency tables (version 47). *Prog. Photovolt. Res. Appl.*, **24**, 3–11.

31 Campbell, P. and Green, M.A. (1987) Light trapping properties of pyramidally textured surfaces. *J. Appl. Phys.*, **62**, 243.

32 Campbell, P. and Green, M.A. (2001) High performance light trapping textures for monocrystalline silicon solar cells. *Sol. Energy Mater. Sol. C*, **65**, 369–375.

33 Spinelli, P. and Polman, A. (2014) Light trapping in thin crystalline Si solar cells using surface Mie scatterers. *IEEE J. Photovolt.*, **4**, 554.

34 Soppe, W., Rieffe, H., and Weeber, A. (2005) Bulk and surface passivation of silicon solar cells accomplished by silicon nitride deposited on industrial scale by microwave PECVD. *Prog. Photovolt. Res. Appl.*, **13**, 551–569.

35 Otto, M., Kroll, M., Kasebier, T., Salzer, R., Tunnermann, A., and Wehrspohn, R.B. (2012) Extremely low surface recombination velocities in black silicon

passivated by atomic layer deposition. *Appl. Phys. Lett.*, **100**, 191603.

36 Glunz, S.W., Rein, S., Lee, J.Y., and Warta, W. (2001) Minority carrier lifetime degradation in boron-doped Czochralski silicon. *J. Appl. Phys.*, **90**, 2397.

37 Macdonald, D. and Geerligs, L.J. (2004) Recombination activity of interstitial iron and other transition metal point defects in p- and n-type crystalline silicon. *Appl. Phys. Lett.*, **85**, 4061.

38 Dingemans, G. and Kessels, W.M.M. (2012) Status and prospects of Al_2–O_3-based surface passivation schemes for silicon solar cells. *J. Vac. Sci. Technol. A*, **30** (4), 040802.

39 De Wolf, S., Descoeudres, A., Holman, Z.C., and Ballif, C. (2012) High-efficiency silicon heterojunction solar cells: a review. *Green*, **2**, 7–24.

40 Spinelli, P., Lenzmann, F., Weeber, A., and Polman, A. (2015) Effect of EVA encapsulation on light trapping in thin-film c-Si solar cells by using plasmonic and Mie nanoscatterers. *IEEE J. Photovolt.*, **5**, 559.

41 Newman, B.K., Sinke, W., and Polman, A. (2014) Light engineering in wafer-based crystalline silicon solar cells. *EU PVSEC* 2014.

42 Ma, F.-J., Duttagupta, S., Shetty, K.-D., Meng, L., Samudra, G.S., Hoes, B., and Peters, I.M. (2014) Two-dimensional numerical simulation of boron diffusion for pyramidally textured silicon. *J. Appl. Phys.*, **116**, 184103.

43 Wagner, H., Steingrube, S., Wolpensinger, B., Dastgheib-Shirazi, A., Chen, R., Dunham, S.T., and Altermat, P.P. (2011) Analyzing emitter dopant inhomogeneities at textured Si surfaces by using 3D process and device simulations in combination with SEM imaging. *IEEE PVSC*, **2011**, 314.

44 Spinelli, P. and Polman, A. (2012) Prospects of near-field plasmonic absorption enhancement in semiconductor materials using embedded nanoparticles. *Opt. Express*, **20**, 641.

45 Coenen, T., van de Groep, J., and Polman, A. (2013) Resonant Mie modes of single silicon nanocavities excited by electron irradiation. *ACS Nano*, **7**, 1689.

46 van de Groep, J. and Polman, A. (2013) Designing dielectric resonators on substrates: combining magnetic and electric resonances. *Opt. Express*, **21**, 26285.

47 Kuznetsov, A.I., Miroshnichenko, A.E., Fu, Y.H., Zhang, J., and Lukyanchuk, B. (2012) Magnetic light. *Sci. Rep.*, **2**, 492.

48 Person, S., Jain, M., Lapin, Z., Saenz, J.J., Wicks, G., and Novotny, L. (2013) Demonstration of zero optical backscattering from single nanoparticles. *Nano Lett.*, **13**, 1806–1809.

49 Kerker, M., Wang, D., and Giles, C.L. (1983) Electromagnetic scattering by magnetic spheres. *J. Opt. Soc. Am.*, **73**, 765–767.

50 Fu, Y.H., Kuznetsov, A.I., Miroshnichenko, A.E., Yu, Y.F., and Lukyanchuk, B. (2013) Directional visible light scattering by silicon nanoparticles. *Nat. Commun.*, **4**, 1527.

51 Ma, W., Yang, C., Gong, X., Lee, K., and Heeger, A.J. (2005) Thermally stable, efficient polymer solar cells with nanoscale control of the interpenetrating network morphology. *Adv. Funct. Mater.*, **15**, 1617–1622.

52 van Lare, M., Lenzmann, F., and Polman, A. (2013) Dielectric back scattering patterns for light trapping in thin-film Si solar cells. *Opt. Express*, **21**, 20738.

53 van Lare, M., Lenzmann, F., and Polman, A. (2015) Dielectric scattering patterns for efficient light trapping in thin-film solar cells. *Nano Lett.*, **15**, 4846.

54 van Lare, M., Yin, G., Polman, A., and Schmid, M. (2015) Light coupling and trapping in ultra-thin Cu(Ga,In)Se_2 solar cells using dielectric scattering patterns. *ACS Nano*, **9**, 9603.

55 Ingenito, A., Luxembourg, S.L., Spinelli, P., Liu, J., Ortiz Lizcano, J.C., Weeber, A., Isabella, O., and Zeman, M. (2015) Optimized metal-free back reflectors for high-efficiency rear c-Si solar cells. *J. Photovolt.*, **6** (1), 1–7.

56 van de Groep, J., Spinelli, P., and Polman, A. (2015) Single-step soft-imprinted large-area nanopatterned anti-reflection coating. *Nano Lett.*, **15**, 4223.

57 Verschuuren, M.A. and van Sprang, H. (2007) 3D photonic structures by sol–gel imprint lithography. 2007 Material Research Society Symposium Proceedings, vol. 1002, pp. N03–N05.